

LA-UR- 11-04178

Approved for public release;  
distribution is unlimited.

<i>Title:</i>	Shock Consolidation Response of CeO <sub>2</sub> Powders
<i>Author(s):</i>	D. Anthony Fredenburg Darcie Dennis-Koller Dana Dattelbaum
<i>Intended for:</i>	Proceedings of the American Physical Society: Shock Compression of Condensed Matter 2011



Los Alamos National Laboratory, an affirmative action/equal opportunity employer, is operated by the Los Alamos National Security, LLC for the National Nuclear Security Administration of the U.S. Department of Energy under contract DE-AC52-06NA25396. By acceptance of this article, the publisher recognizes that the U.S. Government retains a nonexclusive, royalty-free license to publish or reproduce the published form of this contribution, or to allow others to do so, for U.S. Government purposes. Los Alamos National Laboratory requests that the publisher identify this article as work performed under the auspices of the U.S. Department of Energy. Los Alamos National Laboratory strongly supports academic freedom and a researcher's right to publish; as an institution, however, the Laboratory does not endorse the viewpoint of a publication or guarantee its technical correctness.

# SHOCK CONSOLIDATION RESPONSE OF CeO<sub>2</sub> POWDERS

D. Anthony Fredenburg\*, Darcie Dennis-Koller\* and Dana M. Dattelbaum\*

\*WX-9, Shock and Detonation Physics, LANL, Los Alamos, NM 87545

**Abstract.** The compaction response of two distinct morphology CeO<sub>2</sub> powders ranging in size from 300 nm to 10-14  $\mu\text{m}$  are investigated through quasi-static and dynamic compaction experiments. In the quasi-static and low pressure dynamic regimes the high aspect ratio 10-14  $\mu\text{m}$  particles exhibit a measurably stiffer response. However, as pressure increases in the dynamic regime a transition occurs whereby the 10-14  $\mu\text{m}$  powder is more easily compacted than the 300 nm particles, indicating that at low pressures shape effects dominate the compaction response, while at higher pressures particle size dominates. Transmitted wave profiles are examined, and suggest non-equilibrium processes may occur following the initial compaction front. Furthermore, three formulations of the  $P$ - $\alpha$  model are applied to the 300 nm compaction data, and a power law relation is found to yield the best fit with experimental data.

## INTRODUCTION

Metal oxide powders offer a unique platform on which to investigate the shock consolidation and high pressure equation of state response in powder systems. In contrast to metal powders which can compact to solid density at relatively low stresses, many metal oxide powders require much higher stresses to crush up to solid density. As such, the  $P$ - $V$  (pressure-volume) phase space over which metal oxide powders compact is sufficiently large that investigations can be carried out to study the effects of particle morphology (size, shape, etc.) on the shock consolidation and compaction response. This work examines the role of particle morphology on the compaction response of CeO<sub>2</sub> powders.

## MATERIAL

In investigating the shock response of porous systems, it is also desirable, if not required, to have knowledge of the solid equation of state (EOS). A literature review for CeO<sub>2</sub> revealed very little theoretical and/or experimental work had been performed on the shock response of solid CeO<sub>2</sub>, and therefore,

parameters for the solid EOS of CeO<sub>2</sub> had to be determined. The crystallographic and diamond anvil cell compaction data of Duclos et al.[1], which reported values for the bulk modulus and its pressure derivative in terms of a first-order Birch EOS[2], was used to derive the Hugoniot response of CeO<sub>2</sub>. The isothermal compression data of Duclos et al.[1] up to 30 GPa was first fit with the Dugdale-McDonald model[3] to determine the zero pressure Grüneisen parameter  $\gamma_0$ . The isothermal curve was then transformed to a Hugoniot using the previously determined value for  $\gamma_0$  and the Mie-Grüneisen EOS under the assumption that  $\gamma_0/V_0$  remains constant. The resulting parameters for solid CeO<sub>2</sub> used throughout this investigation are given in Table 1.

TABLE 1. Equation of state parameters for solid CeO<sub>2</sub>.

$\rho_0$ (g/cm <sup>3</sup> )	$C_0$ (km/s)	$S$	$\gamma_0$
7.215	5.635	1.257	1.5

Two different morphology CeO<sub>2</sub> powders were investigated, and are shown in Fig. 1. The 300 nm powder (Fig. 1(a)) was obtained from Ocean State Abrasives (West Warwick, RI) and is approximately equiaxed in shape. The larger particles were obtained

from Alfa Aesar (Ward Hill, MA), and particle size was listed from the manufacturer as 10-14  $\mu\text{m}$ . However, it is clear from Fig. 1(b) that the 10-14  $\mu\text{m}$  powder is elongated, with width dimensions measuring much less than the length. Thus, in addition to size differences between the powders, the high aspect ratio of the 10-14  $\mu\text{m}$  powder may also be found to influence the compaction response.

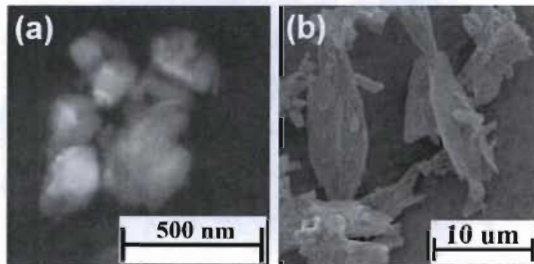


FIGURE 1. SEM micrographs of the two morphology powders showing (a) approximately equiaxed 300 nm and (b) elongated 10-14  $\mu\text{m}$  powder.

## EXPERIMENTAL

The consolidation response of two morphology  $\text{CeO}_2$  powders was investigated through quasi-static and dynamic compression techniques. For quasi-static compression, 5 grams of each powder was loaded into a 25.4 mm ID die and loaded to approximately 120,000 N at a rate of 0.00222 mm/s. Continuous measurements of the load and displacement were used to calculate pressure-density curves for each powder, after subtracting for compliance.

The dynamic response was examined through a series of parallel plate impact experiments. With the exception of the two highest pressure shots, the powders were pre-compressed into a 25.4 mm ID stainless steel cylinder to a nominal initial density of 4.0  $\text{g}/\text{cm}^3$ . The height of the powder was kept constant at 2 mm, and the impactor and driver/base plate materials were both copper. For the highest pressure shots the initial density remained 4.0  $\text{g}/\text{cm}^3$ , but the impactor and driver materials were Kel-F 800, the powder thickness was 6 mm, and the diameter of the pre-compacted specimen was 33 mm. In all experiments the impedance matching technique was used to determine the shocked state in the powder[4]. For this analysis, the velocity of the impacting projectile was measured through a series of shorting pins

or lasers, and the transit time of the shock through the powder was measured using optical velocimetry, both VISAR[5] and PDV[6]. In this configuration, the powder was backed by a 0.5 mm buffer attached to a 16 mm window, where both the buffer and window were PMMA. Velocimetry probes were positioned such that velocity traces were recorded at the powder/buffer and buffer/window interfaces, which allowed for accurate determination of the shock transit time and collection of the transmitted wave profiles through the powder.

## RESULTS

Quasi-static compression of the two powders found that at the upper limit of the pressures investigated (~240 MPa) the 10-14  $\mu\text{m}$  powder compressed to a slightly lower density, and behaved in an overall stiffer manner than the 300 nm powder. Beginning at near ambient pressures, densities ranged from 22-60% and 30-62% for the 10-14 and 300 nm powders, respectively. This suggests that the pressures achieved during quasi-static compaction are sufficiently low such that the initial inefficient packing of the high aspect ratio 10-14  $\mu\text{m}$  powders remains throughout loading.

Results from the dynamic impact experiments, separated on the basis of morphology, are given in Table 2. These impact conditions resulted in pressures in the powders ranging between 0.8 and 12.7 GPa for the 300 nm powder, and between 0.6 and 4.0 GPa for the 10-14  $\mu\text{m}$  powder. Uncertainties in the shock velocity listed encompass tilt and the variation in arrival times measured from separate optical probes. The large uncertainty in shot 56-11-25 is a consequence of recording only one time of arrival measurement as opposed to two in the other 56-series experiments.

The results plotted in  $U_S$ - $u_P$  space are shown in Fig. 2, along with the predicted porous Hugoniot calculated using the parameters in Table 1 and the Mie-Grüneisen EOS with an initial porous density of  $\rho_{00} = 4.0 \text{ g}/\text{cm}^3$ . From Fig. 2 the influence of morphology on the compaction response is easily observed, where at low velocities the 10-14  $\mu\text{m}$  powder responds a manner that is observably more stiff than the 300 nm powder.

As the impact velocity is increased to ~0.4 km/s

**TABLE 2.** Measured impact velocity  $V_{imp}$ , initial density  $\rho_{00}$ , and shock velocity  $U_S$  for the dynamic compaction experiments performed. Shot #'s with \* indicate experiments where impactor and driver/base plate were Kel-F.

Shot #	$V_{imp}$ (km/s)	$\rho_{00}$ (g/cm <sup>3</sup> )	$U_S$ (km/s)
300 nm			
56-11-20	0.219	4.035	1.036 ± 0.055
56-11-19	0.407	4.031	1.306 ± 0.028
56-11-11	0.626	4.040	1.580 ± 0.081
2s-545*	1.799	3.978	2.071 ± 0.012
2s-544*	2.562	3.991	2.648 ± 0.019
10-14 μm			
56-11-26	0.146	4.007	1.066 ± 0.044
56-11-27	0.405	4.011	1.281 ± 0.027
56-11-25	0.726	4.031	1.592 ± 0.283

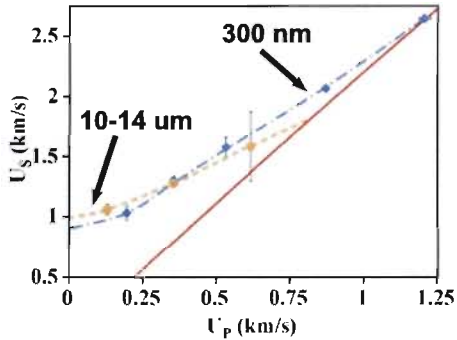


**FIGURE 2.** Measured compaction response of 300 nm (diamonds) and 10-14 μm (circles) powder, along with porous Hugoniot predicted from Mie-Grüneisen analysis (solid line) and best fit curves to the experimental data.

the shock response of the two morphologies is nearly equivalent. At higher impact velocities a transition in stiffness is observed as the 10-14 μm powder transitions from initially stiff to soft, indicating a threshold velocity or pressure has been reached which allows for breakdown of the inefficiently packed networks through comminution and/or deformation of the high aspect ratio powders. From Fig. 2 it appears that the 10-14 μm powder approaches the predicted porous Hugoniot (solid line) at a lower velocity than the 300 nm powder, indicating a lower crush strength for the larger particles. Due to the large error bars of 56-11-25, additional shots are planned to confirm the tran-

sition.

In addition to calculating the Hugoniot response for the two morphology powders, profiles of the compaction wave after it had been transmitted through the powder and into the PMMA buffer/window were also recorded. The transmitted waves for both morphologies had very similar characteristics, and profiles recorded from the 10-14 μm powder are shown in Fig. 3. Analysis of the profiles for all impact velocities showed a sharp rise to peak velocity, followed by a finite amount of curvature prior to the initial region of quasi-steady velocity. It was also found that the time duration of the initial region of quasi-steady velocity increased with increasing impact velocity. Subsequent to the quasi-steady region a reduction in velocity was observed for all impact conditions, where the magnitude of the velocity reduction also increased with increasing impact velocity. The reduction in velocity following the initial compaction front suggests the powder may be in a state of non-equilibrium, where the non-equilibrium processes responsible for the reduction in velocity may be additional compaction, stress relaxation, or some other mechanism.

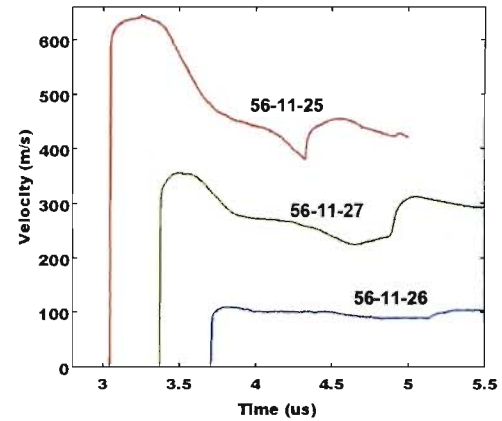


**FIGURE 3.** Transmitted VISAR wave profiles for the 10-14 μm powder showing evolution of the wave profile with increasing impact velocity.

## COMPACTION MODELING

Examining only the experimental data for the 300 nm powder, the ability of three distinct P- $\alpha$  models to capture the measured compaction response was

also investigated. In these models  $\alpha = V/V_S$ , where  $V$  is the volume of the porous material and  $V_S$  is the volume of the solid at the corresponding pressure. Details of the models can be found in [7, 8, 9]. The first model examined was the quadratic formulation of Herrmann[7]:

$$\alpha = 1 + (\alpha_E - 1) \left( \frac{P_S - P}{P_S - P_E} \right)^N \quad (1)$$

where  $\alpha_E$  and  $P_E$  are the distention and pressure at the elastic-plastic transition, and  $P_S$  is pressure at which full compaction occurs. The best fit to Eq. 1 was found with a compaction exponent of  $N = 6.243$ , with  $P_S = 13$  GPa,  $P_E = 0.065$  GPa, and  $\alpha_E = \alpha_0 = 1.804$ . The next model was the rate-independent model of Carroll and Holt[8]:

$$\alpha = 1/(1 - \exp(-3P/2Y)) \quad (2)$$

where  $\alpha$  remains constant below some critical pressure  $P_{crit}$  which is determined from the yield strength  $Y$  of the material[8]. For 300 nm CeO<sub>2</sub>, the yield strength was arbitrarily chosen as the pressure at which the compaction behavior of two morphologies transitions,  $Y = 1.87$  GPa (shot 56-11-19), resulting in a critical pressure of  $P_{crit} = 1.01$  GPa. The third and final  $P$ - $\alpha$  formulation is the power law form suggested by Grady[9]:

$$\alpha = \left( \frac{P_S}{P} \right)^{1/n} \quad (3)$$

where again,  $P_S$  is the crush strength and is set equal to 13 GPa. The best fit to Eq. 3 is found with  $n = 8.582$ . The best fits to the three  $P$ - $\alpha$  fits (Eqns. 1, 2, and 3) are shown in Fig. 4 along with the experimental data and the predicted (fully solidified) porous Hugoniot. From Fig. 4 it is evident that the  $P$ - $\alpha$  relation given by Eq. 3 offers the best fit to the experimental data at both low and high pressures.

## CONCLUSIONS

In examining the quasi-static and shock consolidation behavior of CeO<sub>2</sub> it was found that both size and shape of the powder particles greatly influences the compaction response. At low pressures particle shape effects dominate, as the high aspect ratio 10-14  $\mu\text{m}$  powders were found to exhibit a stiffer response in both the quasi-static and dynamic regimes.

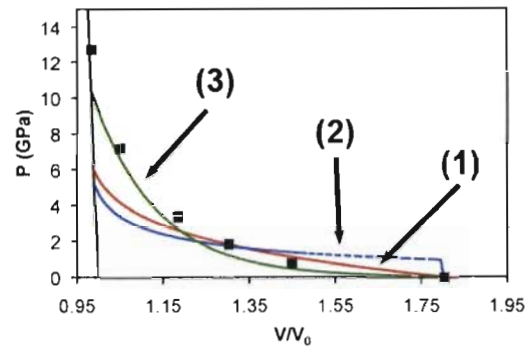


**FIGURE 4.** Compaction data for 300 nm powder, plotted with the predicted porous Hugoniot and three  $P$ - $\alpha$  fits. Numbers in parenthesis indicate equation number.

However, as pressure increases size affects begin to dominate the response, and the larger particles are found to approach the solidified curve at lower overall pressures. With regard to the transmitted wave profiles, similar features are found over the range of impact conditions, and suggest the presence of non-equilibrium processes occurring after passage of the initial wavefront. Furthermore, three separate formulations of the  $P$ - $\alpha$  model were fit to the experimental data, with the power law formulation of Grady[9] offering the best fit to the data.

## ACKNOWLEDGMENTS

## REFERENCES

1. S.J. Duclos, et al., *Phys. Rev. B*. 38 (1988) 7755-7758.
2. F. Birch, *J. Geophys. Res.* 83 (1978) 1257-1268.
3. L. Davison, *Fundamentals of Shock Wave Propagation in Solids*, Springer-Verlag: Berlin, 2008, p. 94.
4. R.G. McQueen, S.P. Marsh, J.W. Taylor, J.N. Fritz, W.J. Carter, in R. Kinslow (Ed.) *High-Velocity Impact Phenomena* Academic Press: New York, 1970.
5. D.H. Dolan, *Foundations of VISAR analysis*, Report: SAND2006-1950, 2006.
6. O.T. Strand, et al., *Rev. Sci. Instrum.* 77 (2006) 083108.
7. W. Herrmann, *J. Appl. Phys.* 40 (1969) 2490-2499.
8. M. Carroll, A. Holt, *J. Appl. Phys.* 43 (1972) 1626-1636.
9. D. Grady, *P-Alpha Compaction of Sand*, unpublished (2007).